Skeletal ossification of Middle Triassic pachypleurosaur *Keichousaurus hui* (Reptilia: Sauropterygia) revealed by Zinc distribution (#114741)

First submission

Guidance from your Editor

Please submit by **25 Mar 2025** for the benefit of the authors (and your token reward) .

Structure and Criteria
Please read the 'Structure and Criteria' page for guidance.

Raw data check
Review the raw data.

Image check
Check that figures and images have not been inappropriately manipulated.

If this article is published your review will be made public. You can choose whether to sign your review. If uploading a PDF please remove any identifiable information (if you want to remain anonymous).

Files

Download and review all files from the materials page.

13 Figure file(s)
1 Table file(s)
1 Other file(s)

Structure and Criteria

Structure your review

The review form is divided into 5 sections. Please consider these when composing your review:

1. **BASIC REPORTING**
2. **EXPERIMENTAL DESIGN**
3. **VALIDITY OF THE FINDINGS**
4. General comments
5. Confidential notes to the editor

🗋 You can also annotate this PDF and upload it as part of your review

When ready submit online.

Editorial Criteria

Use these criteria points to structure your review. The full detailed editorial criteria is on your guidance page.

BASIC REPORTING

Clear, unambiguous, professional English language used throughout.

Intro & background to show context. Literature well referenced & relevant.

Structure conforms to PeerJ standards, discipline norm, or improved for clarity.

Figures are relevant, high quality, well labelled & described.

Raw data supplied (see PeerJ policy).

EXPERIMENTAL DESIGN

Original primary research within Scope of the journal.

Research question well defined, relevant & meaningful. It is stated how the research fills an identified knowledge gap.

Rigorous investigation performed to a high technical & ethical standard.

Methods described with sufficient detail & information to replicate.

VALIDITY OF THE FINDINGS

Impact and novelty is not assessed. Meaningful replication encouraged where rationale & benefit to literature is clearly stated.

All underlying data have been provided; they are robust, statistically sound, & controlled.

Conclusions are well stated, linked to original research question & limited to supporting results.

Standout reviewing tips

The best reviewers use these techniques

Tip	Example
Support criticisms with evidence from the text or from other sources	*Smith et al (J of Methodology, 2005, V3, pp 123) have shown that the analysis you use in Lines 241-250 is not the most appropriate for this situation. Please explain why you used this method.*
Give specific suggestions on how to improve the manuscript	*Your introduction needs more detail. I suggest that you improve the description at lines 57- 86 to provide more justification for your study (specifically, you should expand upon the knowledge gap being filled).*
Comment on language and grammar issues	*The English language should be improved to ensure that an international audience can clearly understand your text. Some examples where the language could be improved include lines 23, 77, 121, 128 – the current phrasing makes comprehension difficult. I suggest you have a colleague who is proficient in English and familiar with the subject matter review your manuscript, or contact a professional editing service.*
Organize by importance of the issues, and number your points	*1. Your most important issue* *2. The next most important item* *3. ...* *4. The least important points*
Please provide constructive criticism, and avoid personal opinions	*I thank you for providing the raw data, however your supplemental files need more descriptive metadata identifiers to be useful to future readers. Although your results are compelling, the data analysis should be improved in the following ways: AA, BB, CC*
Comment on strengths (as well as weaknesses) of the manuscript	*I commend the authors for their extensive data set, compiled over many years of detailed fieldwork. In addition, the manuscript is clearly written in professional, unambiguous language. If there is a weakness, it is in the statistical analysis (as I have noted above) which should be improved upon before Acceptance.*

Skeletal ossification of Middle Triassic pachypleurosaur *Keichousaurus hui* (Reptilia: Sauropterygia) revealed by Zinc distribution

Yi-nuo Wang [1] , **Da-yong Jiang** [Corresp., 1] , **Ryosuke Motani** [2] , **Ming-tao Yao** [1] , **Cheng Ji** [3] , **Zuo-yu Sun** [1] , **Min Zhou** [1]

[1] Department of Geology and Geological Museum, Peking University, Beijing, China

[2] Department of Earth and Planetary Sciences, University of California, Davis, Davis, California, United States

[3] State Key Laboratory of Palaeobiology and Stratigraphy, Nanjing Institute of Geology and Palaeontology, Chinese Academy of Sciences, Nanjing, China

Corresponding Author: Da-yong Jiang
Email address: djiang@pku.edu.cn

The elemental composition was analyzed by applying Micro X-ray fluorescence (Micro-XRF) on seven skeletons of *Keichousaurus hui*, a small pachypleurosaur (Reptilia: Sauropterygia) from the Middle Triassic of Southwest China. The results indicate that the distribution of Zinc (Zn) was notably correlated with the bones of the skeletons and preferentially in certain areas, other than some enriched elements in bones including calcium (Ca), phosphorus (P), and strontium (Sr). Based on the distribution of Zn and its chemical properties, Zn is interpreted as a potential indicator of active ossification in *K. hui.* A comparative analysis of juvenile and subadult specimens reveals distinct patterns of Zn enrichment, reflecting differential bone development across ontogenetic stages. Notably, the Zn distribution in the subadult specimen of *K. hui* suggests the ossification of the tarsals gradually progresses from the centre to the periphery of each tarsal bone, which is consistent with typical endochondral ossification observed in extant reptiles. Furthermore, by integrating morphological features with the observed Zn distribution patterns, we infer that pachyostosis in *K. hui* develops progressively across all stages of growth and development.

Skeletal ossification of Middle Triassic pachypleurosaur *Keichousaurus hui* (Reptilia: Sauropterygia) revealed by Zinc distribution

1 Yi-nuo Wang[1], Da-yong Jiang[1], Ryosuke Motani[2], Ming-tao Yao[1], Cheng Ji[3], Zuo-yu Sun[1], Min
2 Zhou[1]
3
4 [1] Department of Geology and Geological Museum, Peking University, Beijing, China
5 [2] Department of Earth and Planetary Sciences, University of California, Davis, Davis, California,
6   United States
7 [3] State Key Laboratory of Palaeobiology and Stratigraphy, Nanjing Institute of Geology and
8   Palaeontology, Chinese Academy of Sciences, Nanjing, China
9
10
11
12 Corresponding Author:
13 Da-yong Jiang
14 Yiheyuan Street 5, Beijing, 100871, China
15 Email address: djiang@pku.edu.cn
16
17

18 ## Abstract

19 The elemental composition was analyzed by applying Micro X-ray fluorescence (Micro-XRF) on
20 seven skeletons of *Keichousaurus hui*, a small pachypleurosaur (Reptilia: Sauropterygia) from
21 the Middle Triassic of Southwest China. The results indicate that the distribution of Zinc (Zn)
22 was notably correlated with the bones of the skeletons and preferentially in certain areas, other
23 than some enriched elements in bones including calcium (Ca), phosphorus (P), and strontium
24 (Sr). Based on the distribution of Zn and its chemical properties, Zn is interpreted as a potential
25 indicator of active ossification in *K. hui.* A comparative analysis of juvenile and subadult
26 specimens reveals distinct patterns of Zn enrichment, reflecting differential bone development
27 across ontogenetic stages. Notably, the Zn distribution in the subadult specimen of *K. hui*
28 suggests the ossification of the tarsals gradually progresses from the centre to the periphery of
29 each tarsal bone, which is consistent with typical endochondral ossification observed in extant
30 reptiles. Furthermore, by integrating morphological features with the observed Zn distribution
31 patterns, we infer that pachyostosis in *K. hui* develops progressively across all stages of growth
32 and development.

Introduction

Keichousaurus hui is a small pachypleurosaur from the Middle Triassic of the eastern Tethyan region (South China), and serves as the index fossil of the Xingyi Fauna (*Young, 1958*; *Sander, 1989*; *Lin & Rieppel, 1998*; *Rieppel 2000*; *Jiang et al., 2023*). Its ontogenesis, sexual dimorphism, allometric growth, reproductive strategies, and diet preferences have been discussed on the basis of abundant, well preserved, and complete specimens from the Zhuganpo Member of Falang Formation (Ladinian, Middle Triassic) at Xingyi, Guizhou, southwestern China (*Cheng et al., 2004*; *Cheng et a., 2009*; *Fu et al., 2013*; *Motani et al., 2015*; *Xue et al., 2015*; *Liao et al., 2021*; *Li et al., 2023*). Despite these comprehensive investigations, the ossification of *K. hui* bones remains poorly understood (*Li et al., 2023*).

Hard biomineralized tissues, including bones, teeth, and scales, as well as delicate soft tissues such as feathers and skins, can preserve biochemical residues that provide vital insights into the physiology of extinct taxa (*Umarkin-Deratzian et al., 2006*; *Edwards et al., 2011*; *Vitek et al., 2013*; *Qvarnström et al., 2016*; *Lindgren et al., 2018*; *Eriksson et al., 2023*). Among these, hard tissues (e.g., bones) are generally more likely to retain endogenous chemical signatures compared to soft tissues, due to their greater resistance to degradation and diagenetic alteration.

Ossification typically occurs through two distinct processes: direct ossification and indirect ossification, both of which contribute to the formation of normal bone tissue and are regulated a complex interplay of physiological factors (*González et al., 2019*; *Ross et al., 2010*; *Hall et al., 2015*). The trace element, Zn, has been proven to have profound impacts on bone physiology in extant species (*O'Connor et al., 2020*). Zn influences bone ossification either directly, acting on nucleation and mineral growth as a divalent cation, or indirectly, as a cofactor for enzymes like alkaline phosphatase or other metalloenzymes that are integral to the ossification process (*Gomez et al., 1999*). For example, alkaline phosphatase, synthesized by osteoblasts, plays a crucial role in cartilage mineralization and bone formation. This enzyme requires divalent cations like Zn^{2+} as cofactors at the active site to function effectively (*Coleman et al., 1994*; *Gomez et al., 1999*).

The presence of endogenous Zn closely linked to ossification has been well-documented in numerous fossil bones (*Anne et al., 2014,2018*). Zn demonstrates remarkable post-mortem preservation and remains stable throughout the fossilization process, as evidenced by studies on extinct species (*Shinomiya et al., 1998*; *Anne et al., 2014, 2017*). Research on various fossil materials, such as cave hyenas and archosaurs, has revealed a strong correlation between Zn and fossilized bones, which provides critical insight into ossification processes, even among heterochronous species deposited in diverse burial environments (*Anne et al., 2014, 2018*). Consequently, analyzing the distribution of specific elemental markers, such as Zn, can offer valuable information about the physiological state of bone ossification in extinct organisms.

The application of Micro X-ray fluorescence (Micro-XRF) to fossil surfaces, with its high spatial resolution, enables the visualization of entire fossils and facilitates large-scale scanning. Recent studies utilizing non-destructive Micro-XRF on vertebrate fossils and their surrounding matrices have demonstrated its potential not only to complement skeletal anatomy (*Li et al., 2020*; *Schrøder et al., 2022*; *Chen et al., 2023*; *Liu et al., 2024*; *Wang et al., 2024*), but also to

73 enhance our understanding of chemical component in keratinous structures and soft tissues, such
74 as claw sheaths and feathers in *Jianianhualong tengi* (Li et al., 2020) and the trunk
75 of *Mixosaurus panxianensis* (*Wang et al., 2024*). This study aims to apply this method to the
76 skeletal analysis of *K. hui* in order to elucidate bone development and ossification patterns across
77 various ontogenetic stages, including fetal, juvenile, subadult, and adult phases. The aims of this
78 paper are 1) to reveal the elemental distribution (especially Zn) in skeletons of *K.hui*; 2) to
79 explore the implications of the biomarker (Zn) of ossification in *K. hui*; 3) to visualize the
80 ossification patterns of certain bones and different ontogenetic stages, and compare with those in
81 extant species.

Materials & Methods

83   The material for this study includes seven specimens of *K. hui* from Xingyi City, Guizhou,
84 China. Four specimens are housed in the Geological Museum of Peking University (GMPKU),
85 and three are in the Xingyi National Geopark Museum (XNGM). During the preparation process,
86 all specimens were handled with great care to preserve the original biological signals within the
87 bones and the surrounding matrix. Efforts were made to minimize the use of chemical solvents to
88 avoid potential damage to these signals. The specimens were measured with a pair of digital
89 calipers with an accuracy of 0.01 mm using the criteria of Sander (1989). Some parts preserved
90 in a curved posture, such as the neck and trunk, were measured by aligning a cotton thread along
91 the axis and measured by a ruler later. Seven morphological features (*Table 1*), including
92 humerus length (HL), maximum distal width of humerus (MAXDWH), minimum width of
93 humeral shaft (MINWHS), femur length (FeL), snout-vent length (SVL), standard length (SL)
94 and humeral midshaft circumference (HMC), were measured to distinguish their ontogenetic
95 stages and gender following the previous morphology-based classification scheme (*Cheng et al.,*
96 *2009*; *Qin et al., 2014*; *Xue et al., 2015*). Specifically, the HL/FeL is used to estimate whether
97 these specimens have been sexually mature and then gender identification can be quantified in
98 adult individuals by MAXDWH/MINWHS, HL/FeL and HL/SL (*Lin and Rieppel, 1998*; *Cheng*
99 *et al., 2009*) (*Table 1*). According to the criteria established by Lin and Rieppel (1998), adults are
100 defined as those with a HL/FeL ratio greater than 1, while non-adults are characterized by an
101 HL/FeL ratio less than 1(*Table 1*). In adult individuals, genders were assigned following the
102 methodology of Cheng et al. (2009). The diagnostic ratios and their corresponding threshold
103 values are as follows: 1.8 for MAXDWH/MINWHS, 1.1for HL/FeL, and 1.3 for HL/SL (*Cheng*
104 *et al., 2009*). Specimens exhibiting at least one ratio exceeding its respective threshold were
105 classified as male (*Table 1*). Non-adult ontogenetic stages are further subdivided into juveniles
106 (within one year after birth) and subadults (more than one year, but younger than two years) by
107 humeral midshaft circumference (*Table 1*; *Fig. 1*). Based on the data of humeral midshaft
108 circumference and age estimated by bone histology from Li et al. (2023), we have fitted these
109 data and plotted our specimens to facilitate age division (*Fig.1*). However, the humerus of
110 XNGM-WS-31-R22 was broken, so part of the data related is unavailable. GMPKU-P-4317 is a
111 gravid specimen in ventral view whose fetuses cover the four most posterior trunk vertebrae, so
112 the standard length of GMPKU-P-4317 is also unavailable.

113   Elemental maps of the fossil specimens were obtained using the Bruker M6 Jetstream mobile
114   X-ray fluorescence (Micro-XRF) instrument at the Micro-XRF imaging Lab, China University of
115   Geosciences Beijing. The seven skeletons are dorsoventrally preserved and the instrument was
116   calibrated to mitigate height disparities, ensuring that the variance in height at the four corners
117   did not exceed 2mm, thereby meeting the requirements for qualitative imaging. Specific mapping
118   parameters, including acquisition conditions, acquisition time per pixel and total measurement
119   time, are in *Table S1*. Areas of interest, such as the left and right hindlimbs of GMPKU-P-4316,
120   were further investigated by Micro-XRF using higher spatial resolution. The Golden Software
121   Surfer 13 was used to analyze the samples' elemental content data and generate element
122   distribution maps. The XRF mapping is a false-colour image, which only shows the distribution
123   of elements and not their actual concentration.

Results

125   Results are reported here mainly based on three of the specimens that illustrate ontogenetic
126   differences best, namely XNGM WS-30-R43 (juvenile), GMPKU-P-4316 (subadult), and
127   XNGM WS-32-R18 (adult) (*Fig.1*).

Tendency of overall elemental distribution

129   The elemental distribution in *K. hui* demonstrates a pronounced enrichment of elements
130   typically associated with bone, primarily Ca, P, and Sr (*Figs. 2-4*; *Figs. S1-S4*). Additionally,
131   zinc (Zn) shows a strong correlation with skeletal element*s* (*Figs. 2E, 3E, 4E*). Conversely,
132   manganese (Mn), sulfur (S), titanium (Ti), and potassium (K) exhibit higher concentration in the
133   surrounding matrix and are relatively depleted in the skeletal structures (*Fig. S5*).

134   The skeletal structures exhibit a higher Ca content compared to the surrounding matrix,
135   mineralogically consistent with apatite. However, the contrast in Ca-maps is not sufficiently
136   pronounced to clearly delineate the skeletal outlines (e.g., *Figs. 2B, 3B, 4B*). P is primarily
137   distributed in skeletons, thereby revealing the skeletal structures (e.g., *Figs. 2C, 3C, 4C*;).
138   Notably, all seven *K. hui* specimens consistently exhibit distinctly elevated Sr levels throughout
139   the entire skeleton, providing exceptional anatomical clarity (e.g., *Figs. 2D, 3D, 4D*). The Sr-
140   maps demonstrate a higher contrast compared to the Ca-maps and P-maps, suggesting that they
141   have the best potential for distinguishing bones from the matrix.

142   The distribution of Zn in *K. hui* varies significantly among the seven specimens. In three
143   specimens—XNGM WS-30-R43 (*Fig. 2E*), GMPKU-P-4316 (*Fig. 3E*), and XNGM WS-32-R18
144   (*Fig. 4E*)—Zn shows a strong correlation with skeletal structures, but with distinct distribution
145   patterns in each specimen. In contrast, the remaining four specimens do not exhibit elevated Zn
146   levels in the skeletal regions (*Figs. S1E, S2E, S3E, S4E*). Given this variability, the Zn
147   distribution in the three specimens displaying skeletal enrichment is described in greater detail
148   below.

Elemental distribution in XNGM WS-30-R43, GMPKU-P-4316 and XNGM WS-32-R18

Elemental distribution in XNGM WS-30-R43

152   XNGM WS-30-R43 is a well-preserved juvenile individual in ventral view (*Fig. 2*). Zn is

153 primarily concentrated in the skull and along the axial skeleton, particularly in the cervical
154 vertebrae and caudal vertebrae (*Figs. 2E,2F*). Notably, Zn enrichment is also observed in the
155 proximal ends and shafts of the dorsal ribs, as well as both the proximal and distal ends of the
156 long bones in the limbs.

157 **Elemental distribution in GMPKU-P-4316**

158   GMPKU-P-4316 is a subadult individual exposed in ventral view (*Fig. 3*). The Zn-map shows
159 that the distribution of Zn is closely related to the skeletal structure, with higher Zn content
160 observed in specific bones such as the parietal, carpals, tarsals, proximal ends and shafts of the
161 dorsal and caudal ribs. Notably, the proximal ends and shafts of dorsal and caudal ribs shows
162 distinct Zn enrichment compared to the rest of the ribs, forming a bilaterally symmetrical pattern
163 along the dorsal and caudal vertebrae *(Fig. 3E, 3F)*. Zn distribution around the tarsals is
164 particularly noteworthy, showing a nearly circular pattern consistent with the bone shape (*Figs.
165 5-6*). According to the complete outline of the tarsals in the light photo and Sr-map (since Sr can
166 clearly delineate bone morphology, we use Sr-maps here to reveal the structure), high Ca and P
167 concentrations are concentrated primarily in the centers of the astragalus and calcaneum (*Figs.
168 6H, 6I*; *7H, 7I*). In contrast, Zn distribution is roughly complementary to Ca and P, extending
169 slightly beyond the skeletal outline of the tarsals (*Figs. 6L, 6M*; *7L, 7M*). The Zn-map also
170 reveals the possible shape of the fourth distal tarsal (dt4). In the left hindlimb, the dt4 is visible in
171 the Zn-map, Sr-map, and light photo, appearing as a subround area between the astragalus and
172 calcaneum (*Fig. 6G, 6J, 6K*), but absent in the Ca-map or P-map (*Fig. 6H, 6I*). Moreover, this
173 subround Zn-enriched area is larger than those observed in the Sr-map and light photo (*Fig. 6G,
174 6J, 6K*). In the right hindlimb, the dt4 is only visible in the Zn-map (*Fig. 7J*) and not in other
175 maps (*Fig. 6H, 6I*). Additionally, the Zn content in the metatarsal close to the tarsal gradually
176 diminishes from the proximal towards the distal end in both hindlimbs (*Figs. 6F, 6K*; *7J, 7K*).

177 **Elemental distribution of XNGM WS-32-R18**

178   XNGM WS-32-R18 is an adult individual in dorsal view, with part of the tail missing (*Fig. 4*).
179 Zn also appears to be enriched in some bones. Interestingly, Zn accumulates at the articular
180 surfaces where each centrum connects with the previous one (*Fig. 4E*). The proximal ends of the
181 dorsal and caudal ribs exhibit distinct Zn enrichment compared to the rest of the ribs, and the
182 proximal and distal ends of the long bones in the limbs are also notably enriched in Zn. The two
183 dark parts in the trunk region covered by the dorsal ribs and the gastral ribs also show the high
184 level of Zn (*Fig. 4E*).

185 # Discussion

186 **Preservation mechanisms of Ca, P, Sr, Zn within fossil bones**

187   Changes in the elemental composition of fossil bones can occur during two distinct periods:
188 first, during the organism's lifetime, and second, during the fossilization process (*Piga et al.,
189 2011*). Throughout fossilization, the preservation mechanisms of various elements differ due to a
190 complex interplay of chemical, physical, and environmental factors (*Parker & Toots, 1970*;
191 *Dumont et al., 2009*; *Piga et al., 2011*). Calcium hydroxyapatite ($Ca_{10}(PO4)_6(OH)_2$), the primary
192 inorganic content of bones, has the flexibility of the lattice for replacements at every site within

193 the mineral structure. This flexibility enables the replacement of Ca^{2+}, PO_4^{3-}, and OH^- ions with
194 other ions, facilitating both the uptake and loss of elements within the bones (*Miyaji et al., 2005*;
195 *Trueman et al. 2008*).

196   Despite some inevitable loss during fossilization, Ca and P are highly tenacious and stable,
197 remaining the predominant constituents in fossil bones (*Pan & Fleet, 2002*). For instance, in the
198 bones of the Middle Triassic marine reptile *Mixosaurus panxianensis*, Ca accounts for 68.86
199 wt% to 71.11 wt%, and P ranges from 6.67 wt % to 8.05 wt % (*Wang et al., 2024*). A similar
200 pattern has been consistently documented across a wide range of fossil records (*Li et al., 2020*; *Li
201 et al., 2024*), and this trend is also observed in seven specimens of *K.hui* analyzed in this study
202 (e.g., *Figs. 1B-C*; *2B-C*; *3B-C*; *4B-C*). The enrichment of Sr in fossils occurs both during the
203 organism's lifetime and through the fossilization process. Sr concentrations are higher in
204 seawater than in freshwater, resulting in marine organisms typically exhibiting higher Sr content
205 that is strongly correlated with the Sr levels in their environment (*Rosenthal, 1970*). Sr
206 incorporates into the bones during fossilization through substitution processes, leading to further
207 enrichment, reflected by the elevated Sr content observed in the seven *K.hui* specimens (*e.g.,
208 Figs. 1D*; *2D*; *3D*; *4D*) (*Gueriau et al., 2018*).

209   However, the preservation of Zn in fossil bones presents significant challenges, as some
210 degree of Zn loss is inevitable during the fossilization and preparation processes. First, in living
211 organisms, Zn is present in much lower concentrations and is unevenly distributed within bones
212 compared to the abundant endogenous Ca and P (*Goodwin et al., 2007*; *Wang et al., 2024*).
213 Second, postmortem Zn loss is an unavoidable consequence of diagenetic processes, including
214 demineralization (*Dean et al., 2023*). Micro-XRF scans of *Mixosaurus panxianensis* have
215 revealed a pattern of Zn diffusion, with Zn concentrations gradually decreasing from the trunk
216 region toward the surrounding matrix (*Wang et al., 2024*). Finally, the fossil preparation process
217 can also alter the original distribution of Zn, despite efforts to minimize such impacts. Physical
218 friction during matrix removal can damage the original Zn signal, and the use of solvents such as
219 water or acetone during preparation can lead to Zn loss. Notably, Zn^{2+} exhibits high solubility in
220 water, increasing the likelihood of its removal during preparation (*Mou, 1999*). As a result,
221 among the seven *K.hui* specimens analyzed, only three retained a relatively intact original Zn
222 signal (*Figs. 2E; 3E; 4E*). The remaining specimens failed to preserve this signal due to factors
223 related to fossilization or preparation.

224 **Origin of Zn in *Keichousaurus hui***

225   The robust correlation between Zn intensity and bone morphology in specimens XNGM WS-
226 30-R43, GMPKU-P-4316, and XNGM WS-32-R18 suggests that the observed Zn enrichment in
227 these fossilized bones is endogenous (*Figs. 2E, 3E, 4E*). This interpretation is supported by
228 several lines of evidence. Firstly, unlike other bone-related elements such as Ca, P, and Sr, which
229 are uniformly distributed throughout the skeletal structures, Zn is localized to specific skeletal
230 regions. For example, Zn is concentrated in areas like the periphery of tarsal bones in *K.hui*
231 (*Figs.6 ;7*). Zn exhibits an uneven distribution within the bones of extant and extinct species,
232 predominantly localizing in regions between mineralized and unmineralized zones of osteons, as
233 well as at the ossification front where active calcification occurs (*Bradleya et al., 2007*; *Anne et*

234 *al., 2014*). For instance, synchrotron microfocus X-ray analysis of the forelimbs of one-day-old
235 mice supports this pattern, demonstrating Zn enrichment across all skeletal elements, including
236 both cartilage and bone (*Fig. 8D*). Peak concentrations are observed at the developing edges of
237 bones, a distribution pattern strikingly similar to that observed in *K. hui* (*Fig. 8D*) (*Anne et al.,*
238 *2017*). Secondly, Zn content in the surrounding pelitic limestone is significantly lower than that
239 detected in the bones of the three specimens, indicating a lack of exogenous Zn. Thirdly, there is
240 no evidence to suggest that Zn could have been transferred by aqueous fluids in this system.
241 Mineralogical experiments indicate that substituting exogenous Zn for Ca in hydroxyapatite is
242 relatively challenging (*Miyaji et al., 2004*). This contrasts with the physiological incorporation of
243 Zn into bone, suggesting that Zn from groundwater is unlikely to enter bones through
244 substitution processes.
245   Hence, the Zn enrichment is more likely to be endogenic, i.e., the Zn was accumulated when
246 these *K.hui* were still alive. The distribution of Zn reflects the original organism's chemical
247 remains rather than taphonomic artifacts added during fossilization, despite the preservation
248 mechanism remains unclear.

249 The different ossification patterns in juvenile and subadult individuals

250   The distribution patterns of Zn, especially the enrichments in the XNGM WS-30-R43 and
251 GMPKU-P-4316(*Figs. 2-3*), indicates active ossification in *K. hui*. XNGM WS-30-R43, a
252 juvenile specimen, exhibits higher Zn levels predominantly in the axial skeleton compared to the
253 limbs, suggesting that the axial bones develop more rapidly or earlier than the limb bones at this
254 ontogenetic stage (*Fig. 2E*). GMPKU-P-4316, a subadult individual, displays high Zn levels in
255 scattered areas such as the carpals, tarsus, parietal, proximal ends of dorsal ribs, and caudal ribs
256 (*Fig. 3*), suggesting active ossification in these regions during the subadult stage. Notably, Zn
257 enrichment in the parietal bone indicates that this region was actively ossifying, with the parietal
258 opening gradually closing (*Figs. 3E,3F*). Similarly, the high Zn content in the ends and shafts of
259 dorsal ribs implies continued ossification in these regions (*Figs. 3E,3F*). These findings align
260 with previous descriptions of subadult *K. hui* by Lin & Rieppel (1998) and Qin et al. (2014),
261 which highlight rapid ossification of sexually dimorphic limb elements (e.g., carpals and tarsus),
262 expansion of dorsal rib ends, and closure of the parietal opening. The observed Zn distribution in
263 GMPKU-P-4316 corroborates these developmental patterns.
264   In subadult specimens, Zn enrichment is notably absent in the neck and certain cranial regions,
265 with a sharp demarcation line separating these areas from others, suggesting an abrupt rather
266 than gradual transition (*Fig. 3E*). Microscopic observations revealed that the specimen had been
267 somewhat excessive prepared, potentially resulting in the loss of original Zn signals.
268 Alternatively, Zn may not have been preserved in these regions during fossilization, as discussed
269 earlier, due to the challenges associated with its preservation. Consequently, it cannot be
270 definitively concluded that the neck of subadult individuals lacked Zn enrichment. It is plausible
271 that the neck, like the tail, underwent active ossification, consistent with previous allometric
272 growth analyses (*Xue et al., 2015*). Unfortunately, this detail is not reflected in the Zn
273 distribution maps, despite meticulous fossil preparation efforts.
274   The Zn-maps of XNGM WS-30-R43 and GMPKU-P-4316 reveal distinct ontogenetic

275 patterns of ossification, indicating rapid developmental in both juvenile and subadult individuals
276 (*Fig.5A*). In the juvenile period, ossification mainly occurred in the axial bones and the limbs,
277 while the actively ossifying bones in subadult individual are in the limbs (*Figs. 2E,2F*).

278 **Ossification patterns of tarsus in *Keichousaurus hui* and comparison with extant**
279 **species**

280   The ossification pattern of the tarsus in *K.hui,* as indicated by the distribution of Zn,
281 demonstrates a progressive progression from the centre to the periphery (*Fig. 5B*). This pattern
282 aligns closely with the highly conserved ossification sequence observed in extant reptiles, which
283 exemplifies typical endochondral ossification (*Rieppel, 1991*). In this pattern, the ossification
284 center of the tarsal bones initially appears as relatively small regions within larger cartilage
285 primordia and subsequently expand radially from the centre to the periphery of each tarsal
286 element (*Hemo et al., 2019*). In early postnatal laboratory mice, ossification centre is also in the
287 cartilage primordia and gradually expanded *(Patton & Kaufman, 1995*) (*Fig.8G*). Similarly,
288 in *Cyrtodactylus pubisulcus* (Gekkonidae), the ossification centers similarly originate within the
289 cartilage primordia and undergo gradual expansion over time, and the tarsal ossification
290 sequence begins with the astragalus, followed by the calcaneum, and then the dt4 bone (dt4). In
291 terms of size, the tarsal elements follow the order astragalus > calcaneum > dt4 (*Rieppel, 1992*)
292 (*Fig. 8F*).

293   Notably, in the astragalus and calcaneum of GMPKU-P-4316, Zn exhibits higher
294 concentrations in the peripheries compared to the centres (*Figs. 6-7*), suggesting that the
295 peripheries were actively undergoing ossification while the centres may have already completed
296 ossification. Additionally, the concentrations of Ca and P in the centres of the astragalus and
297 calcaneum exceed those in the peripheries, complementing the distribution pattern of Zn (*Figs.*
298 *6L,6M;7L,7M*). This further supports the inference that the degree of calcification is more
299 advanced in the centers than in the peripheries. A partial extension of Zn is observed beyond the
300 supporting bony elements, distributed along the sub-round bone margin in hindlimb (*Figs.*
301 *6N,7N*), which may represent biological residues from the bone development process.
302 Furthermore, the right hindlimb of GMPKU-P-4316 displays a subcircular area in the Zn-map
303 (*Fig. 7J*) between the astragalus and calcaneum, which is absent in the light photo, Ca-map, P-
304 map, and Sr-map (*Figs. 7F-7I*). This subcircular region in the Zn map may correspond to the
305 biological remains of the dt4, which appears not to have ossified yet. By comparing the
306 elemental distributions between the centers and peripheries, we can gain deeper insights into the
307 ossification process of the tarsus in *K. hui*. This analysis supports the conclusion that the
308 ossification pattern of the tarsus in *K. hui* follows a gradual progression from the center to the
309 periphery (*Fig. 5B*).

310   According to the element maps, the astragalus exhibits a larger relative area enriched in Ca
311 and P compared to the calcaneum, indicating that the extent of ossification is more advanced in
312 the astragalus than in the calcaneum (*Figs. 6L,6M;7L,7M*). Morphological observations further
313 reveal that the irregular shape of the calcaneum suggests incomplete ossification. Therefore, the
314 sequence of tarsal ossification in *K. hui* can be inferred as astragalus, calcaneum, and dt4, which
315 aligns with the ossification pattern observed in certain members of Gekkonidae (*Rieppel, 1992*).

The ossification of ribs in *Keichousaurus hui*

316
317 Pachyostosis, a non-pathological bone hypertrophy, is observed in a wide array of taxa
318 adapted to marine environments, irrespective of their phylogenetic relationships (*Houssaye,*
319 *2009*). The increase in skeletal mass plays the functional role of ballast for buoyancy control and
320 hydrostatic regulation of body trim (*Ricqlès & Buffrénil 2001*; *Houssaye et al., 2009*). The
321 Middle Triassic pachypleurosaurs, which inhabited shallow epicontinental marine habitats and
322 intraplatform basins, display pachyostosis in most elements of the presacral axial skeleton (*Sues*
323 *1987*; *Rieppel & Kebang 1995*; *O'Keefe et al. 1999*). In *K. hui*, pachyostosis is particularly
324 evident in the dorsal region, where the ribs and vertebrae are thickened (Yong, 1958).
325 In the juvenile individual (XNGM WS-30-R43), the shafts of dorsal ribs exhibit elevated Zn
326 content (*Fig. 2E,2F*), suggesting active ossification in these regions. Similarly, the subadult
327 individual (GMPKU-P-4294) shows Zn enrichment in the shafts of dorsal ribs, though the areas
328 with high Zn content are less extensive compared to the juvenile (*Fig. 3E,3F*). Notably,
329 pachyostosis is not apparent in either the juvenile or subadult specimens (*Fig. 2B–2D; 3B–3D*).
330 The adult individual exhibits significant zinc (Zn) enrichment in the rib shafts, suggesting that
331 ossification is still ongoing, while pachyostosis is clearly evident (*Figure 4E*).
332 Previous morphological studies have indicated that pachyostosis is absent in *K. hui* embryos
333 (*Yong, 1958*). Our observations of juvenile and subadult individuals also show no clear signs of
334 pachyostosis, but the pachyostosis is apparent in adult individual. In addition, the distribution of
335 Zn highlights active ossification in the shafts of the dorsal ribs in juvenile, subadult and adult
336 individuals. Integrating these morphological features with Zn distribution patterns, we infer that
337 pachyostosis in *K. hui* develops progressively from embryonic stages to adulthood.

The advantage of Zn revealing the ossification information in fossils

338
339 Zn, preserved *in situ* over deep time, enables the identification of active ossification sites
340 related to ontogenetic stages, particularly in non-adult extinct organisms. Moreover, the
341 macroscopic enrichment of Zn can elucidate the ossification pattern of different ontogenetic
342 individuals, providing more information about growth pattern.
343 Comparative anatomy and bone histology techniques have been used to reconstruct the
344 ossification patterns in fossil marine reptiles (*Klein & Sander, 2008*; *Scheyer et al., 2010*).
345 However, comparative anatomy as direct investigation is usually hampered by preservative
346 conditions and the number of specimens (*Horner & Weishampel, 1996*). Paleohistology which
347 can provide an independent assessment of the age or ontogenetic stage of extinct species based
348 on developmental records in skeletal tissues, is a destructive method and unsuitable for rare
349 fossil specimens (*Klein & Sander, 2008*). Hence, XRF mapping of Zn presents a novel, non-
350 destructive method for addressing ossification, especially in precious specimens, offering
351 additional insights into ossification patterns in fossils.

Conclusion

352
353 This study utilized Micro-XRF scanning to analyze seven *Keichousaurus hui* specimens at
354 different ontogenetic stages. In addition to the conventional elements, the presence of Zn was
355 identified, indicating active ossification in *K. hui*. The enrichment of Zn indicates ossification

356 patterns at different ontogenetic stages. Moreover, the ossification process of the tarsal, gradual
357 ossification from the centre to the periphery like extant reptiles, is also revealed by high Zn
358 concentration. In addition, through the integration of morphological characteristics with the
359 distribution of Zn, we deduce that pachyostosis in *K. hui* develops progressively throughout the
360 organism's developmental stages. The distribution of Zn revealed by Micro-XRF offers an
361 innovative technique for investigating ossification, especially advantageous for analyzing
362 delicate or irreplaceable specimens, while enhancing our comprehension of ossification
363 processes in fossils.

Acknowledgements

Reference

372 **Agusa T, Matsumoto T, Ikemoto T, Anan Y, Kubota R, Yasunaga G, Kunito T, Tanabe S,**
373 **Ogi H, Shibata Y.** 2005. Body distribution of trace elements in black-tailed gulls from Rishiri
374 Island, Japan: age-dependent accumulation and transfer to feathers and eggs. *Environmental*
375 *Toxicology and Chemistry* 24(9): 2107-2120 DOI: 10.1897/04-617r.1.
376 **Alexander B, Daulton TL, Genin GM, Lipner J, Pasteris JD, Wopenka B, Thomopoulos S.**
377 2012.The nanometre-scale physiology of bone: steric modelling and scanning transmission
378 electron microscopy of collagen–mineral structure. *Journal of the Royal Society Interface* 9(73):
379 1774-1786 DOI: 10.1098/rsif.2011.0880.
380 **Anné J, Edwards NP, Wogelius RA, Tumarkin-Deratzian AR, Sellers WI, van Veelen A,**
381 **Bergmann U, Sokaras D, Alonso-Mori R, Ignatyev K, Egerton VM, Manning PL.**2014.
382 Synchrotron imaging reveals bone healing and remodelling strategies in extinct and extant
383 vertebrates. *Journal of the Royal Society Interface* 11(96): 20140277
384 DOI: 10.1098/rsif.2014.0277.
385 **Anné J, Wogelius RA, Edwards NP, Van Veelen A, Ignatyev K, Manning PL.** 2016.
386 Chemistry of bone remodelling preserved in extant and fossil Sirenia. *Metallomics* 8(5): 508-513
387 DOI: 10.1039/c5mt00311c.
388 **Anné J, Edwards NP, Van Veelen A, Egerton VM, Manning PL, Mosselmans JFW, Parry**
389 **S, Sellers WL, Buckley M, Wogelius RA.** 2017.Visualisation of developmental ossification
390 using trace element mapping. *Journal of Analytical Atomic Spectrometry* 32(5): 967-974
391 DOI: 10.1039/C7JA00042A.
392 **Bedwal RS, Bahuguna A.** 1994. Zinc, copper and selenium in reproduction. *Experientia* 50:
393 626-640 DOI: 10.1007/BF01952862.
394 **Bradley DA, Moger CJ, Winlove CP.** 2007. Zinc deposition at the bone–cartilage interface in

395 equine articular cartilage. *Nuclear Instruments and Methods in Physics Research* 580(1): 473-
396 476 DOI: 10.1016/j.nima.2007.05.143.
397 **Bergmann U, Morton RW, Manning PL, Sellers WI, Farrar S, Huntley KG, Wogelius RA,**
398 **Larson P.** 2010.Archaeopteryx feathers and bone chemistry fully revealed via synchrotron
399 imaging. *Proceedings of the National Academy of Sciences* 107(20): 9060-9065
400 DOI: 10.1073/pnas.1001569107.
401 **Coleman JE.** 1992.Structure and mechanism of alkaline phosphatase. *Annual review of*
402 *biophysics and biomolecular structure* 21(1): 441-483
403 DOI: 10.1146/annurev.bb.21.060192.002301.
404 **Cheng Y-N, Wu X-C, Ji Q.** 2004. Triassic marine reptiles gave birth to live young. *Nature*
405 432(7015): 383-386 DOI: 10.1038/nature03050.
406 **Cheng Y-N, Holmes R, Wu X-C, Alfonso N.** 2009. Sexual dimorphism and life history of
407 *Keichousaurus hui* (Reptilia: Sauropterygia). *Journal of Vertebrate Paleontology* 29(2): 401-408
408 DOI: 10.1671/039.029.0230.
409 **Dumont M, Zoeger N, Streli C, Wobrauschek P, Falkenberg G, Sander PM, Kaysser-**
410 **Pyzalla AR.**2008. Synchrotron XRF analyses of element distribution in fossilized sauropod
411 dinosaur bones. *Powder Diffraction* 24(2): 130-134 DOI: 10.1154/1.2951712
412 **Dean MC, Garrevoet J, Van Malderen SJM, Santos F, Mirazón Lahr M, Foley R, Le**
413 **Cabec A.** 2023.The distribution and biogenic origins of zinc in the mineralised tooth tissues of
414 modern and fossil hominoids: implications for life history, diet and taphonomy. *Biology* 12(12):
415 1455 DOI: 10.3390/biology12121455.
416 **Erickson GM, Currie PJ, Inouye BD, Winn AA.** 2006.Tyrannosaur life tables: an example of
417 nonavian dinosaur population biology. *Science* 313(5784): 213-217
418 DOI: 10.1126/science.1125721.
419 **Edwards NP, Barden HE, van Dongen BE, Manning PL, Larson PL, Bergmann U, Sellers**
420 **WI, Wogelius RA.** 2011.Infrared mapping resolves soft tissue preservation in 50 million year-
421 old reptile skin. *Proceedings of the Royal Society B: Biological Sciences* 278(1722): 3209-3218
422 DOI: 10.1098/rspb.2011.0135.
423 **Green J, Kleeman CR.** 1991.The role of bone in the regulation of systemic acid-base balance.
424 *Calcium-Regulating Hormones II* 91: 61-76 DOI: 10.1038/ki.1991.2.
425 **González MS.** 2019.Skeletal cartilage and bone formation, composition, and function in small
426 mammals, birds, and reptiles. *Veterinary Clinics: Exotic Animal Practice* 22(2): 123-134
427 DOI: 10.1016/j.cvex.2019.01.001.
428 **Gomez S, Rizzo R, Pozzi-Mucelli M, Bonucci E, Vittur F.** 1999.Zinc mapping in bone tissues
429 by histochemistry and synchrotron radiation–induced X-ray emission: correlation with the
430 distribution of alkaline phosphatase. *Bone* 25(1): 33-38 DOI: 10.1016/s8756-3282(99)00102-7.
431 **Gueriau P, Jauvion C, Mocuta C.** 2018. Show me your yttrium, and I will tell you who you
432 are: implications for fossil imaging. *Palaeontology* 61(6):981-990 DOI:
433 10.1111/pala.12377.
434 **Goodwin MB, Grant P G, Bench G, Holroyd PA.** 2007.Elemental composition and diagenetic
435 alteration of dinosaur bone: distinguishing micron-scale spatial and compositional heterogeneity

436 using PIXE. *Palaeogeography, Palaeoclimatology, Palaeoecology* 253(3-4): 458-476 **DOI:**

437 10.1016/j.palaeo.2007.06.017.

438 **Honda K, Fujise Y, Tatsukawa R, Miyazaki N.** 1984. Composition of chemical components in

439 bone of striped dolphin, Stenella coeruleoalba: distribution characteristics of heavy metals in

440 various bones. *Agricultural and biological chemistry* 48(3): 677-683 DOI:

441 10.1080/00021369.1984.10866136.

442 **Horner JR, Weishampel DB.** 1996. Correction: a comparative embryological study of two

443 ornithischian dinosaurs. *Nature* 383(6595): 103-103 DOI: 10.1038/332256a0.

444 **Hollocher TC, Chin K, Hollocher KT, Kruge MA.** 2001.Bacterial residues in coprolite of

445 herbivorous dinosaurs: role of bacteria in mineralization of feces. *Palaios* 16(6): 547-565 DOI:

446 10.1669/0883-1351(2001)016<0547:BRICOH>2.0.CO;2.

447 **Houssaye A.** 2009. "Pachyostosis" in aquatic amniotes: a review. *Integrative Zoology* 4(4): 325-

448 340DOI: 10.1111/j.1749-4877.2009.00146.x.

449 **Hemo Y, Gigi R, Wientroub S.** 2019. Delayed ossification and abnormal development of tarsal

450 bones in idiopathic clubfoot: should it affect bracing protocol when using the Ponseti method?

451 *Journal of Children's Orthopaedics* 13(3): 265-270 DOI: 10.1302/1863-2548.13.190080.

452 **Jiang D-Y, Zhou M, Motani R, Tintori A, Fraser NC, Huang J-D, Rieppel O, Ji C, Fu W-L,**

453 **Sun Z-Y, Lu H.**2023. Emergence and ecological transition of the Mesozoic marine reptiles:

454 Evidence from the Early Triassic Chaohu and the Middle Triassic Xingyi Faunas.

455 *Palaeogeography, Palaeoclimatology, Palaeoecology* 628: 111750

456 DOI: 10.1016/j.palaeo.2023.111750.

457 **Klein N, Sander M.** 2008.Ontogenetic stages in the long bone histology of sauropod dinosaurs.

458 *Paleobiology* 34(2): 247-263 DOI: 10.1666/0094-8373(2008)034[0247:OSITLB]2.0.CO;2.

459 **Li Q, Liu J, Klein N, Nakajima Y, Sander PM.** 2023.Puberty in a Mesozoic reptile. *Current*

460 *Biology* 33(14): 3011-3016 DOI: 10.1016/j.cub.2023.05.073.

461 **Lin K, Rieppel O.**1998. Functional morphology and ontogeny of *Keichousaurus hui* (Reptilia,

462 Sauropterygia). *Fieldiana Geol.* 39, 1–35 DOI: 10.5962/bhl.title.5174.

463 **Lindgren J, Sjövall P, Thiel V, Zheng W, Ito S, Wakamatsu K, Hauff R, Kear BP, Engdahl**

464 **A, Alwmark C, Eriksson ME, Jarenmark M, Sachs S, Ahlberg PE, Marone F, Kuriyama T,**

465 **Gustafsson O, Malmberg P, Thomen A, Rodríguez-Meizoso I, Uvdal P, Ojika M,**

466 **Schweitzer MH.**2018. Soft-tissue evidence for homeothermy and crypsis in a Jurassic

467 ichthyosaur. *Nature* 564(7736): 359-365 DOI: 10.1038/s41586-018-0775-x.

468 **Li J-H, Pei R, Teng F-F, Qiu H, Tagle R, Yan Q-Q, Wang Q, Chu X-L, Xu X.** 2020.Micro-

469 XRF study of the troodontid dinosaur *Jianianhualong tengi* reveals new biological and

470 taphonomical signals. *Atomic Spectroscopy* 42(1):1-11 DOI:10.46770/AS.2021.01.001.

471 **Liu Y-C, Ji Q, Wang X-R, O'Connor JK, Guo B, Ren T-L, Yin T-T, Wang Y-B.**

472 2024.Micro-XRF Mapping Elucidates the Taphonomy of Two Early Cretaceous Paravian Fossils

473 from Western Liaoning, China. *Atomic Spectroscopy* 45(2):123-131 DOI:

474 10.46770/AS.2024.033.

475 **Motani R, Jiang D-Y, Rieppel O, Xue Y-F, Tintori A.**2015. Adult sex ratio, sexual

476 dimorphism and sexual selection in a Mesozoic reptile. *Proceedings of the Royal Society B:*

477 *Biological Sciences* 282(1815): 20151658 DOI: 10.1098/rspb.2015.1658.

478 **Miyaji F, Kono Y, Suyama Y.** 2005.Formation and structure of zinc-substituted calcium
479 hydroxyapatite. *Materials Research Bulletin* 40(2): 209-220
480 DOI: 10.1016/j.materresbull.2004.10.020.

481 **Mou B-L.** 1999.*Element Ceochemistry*. Beijing: Peking University Press, 128.

482 **O'Connor JP, Kanjilal D, Teitelbaum M, Lin SS, Cottrell JA.** 2020.Zinc as a therapeutic
483 agent in bone regeneration. *Materials* 13(10): 2211 DOI: 10.3390/ma13102211.

484 **Parker RB, Toots H.** 1970. Minor elements in fossil bone. *Geological Society of America*
485 *Bulletin* 81(3): 925-932 DOI: 10.1130/0016-7606(1970)81[925:MEIFB]2.0.CO;2.

486 **Patton JT, Kaufman MH.** 1995.The timing of ossification of the limb bones, and growth rates
487 of various long bones of the fore and hind limbs of the prenatal and early postnatal laboratory
488 mouse. *Journal of anatomy* 186(Pt 1): 175 PMCID: PMC1167283.

489 **Pan Y, Fleet ME.** 2002.Compositions of the apatite-group minerals: substitution mechanisms
490 and controlling factors. *Reviews in mineralogy and geochemistry* 48(1): 13-49 DOI:
491 10.2138/rmg.2002.48.2.

492 **Piga G, Santos-Cubedo A, Brunetti A, Piccinini M, Malgosa A, Napolitano E, Enzo S .**
493 2011. A multi-technique approach by XRD, XRF, FT-IR to characterize the diagenesis of
494 dinosaur bones from Spain. *Palaeogeography, Palaeoclimatology, Palaeoecology* 310(1-2): 92-
495 107 DOI: 10.1016/j.palaeo.2011.05.018.

496 **Qin Y-J, Yu M-Y, Luo Y-M.** 2014.Ontogeny of *Keichousaurus hui*. *Guizhou Geology* 31(3):
497 210-214 DOI: 10.3969/j.issn.1000-5943.2014.03.009.

498 **Qvarnström M, Niedźwiedzki G, Žigaitė Ž.** 2016. Vertebrate coprolites (fossil faeces): an
499 underexplored Konservat-Lagerstätte. *Earth-Science Reviews* 162: 44-57 DOI:
500 10.1016/j.earscirev.2016.08.014.

501 **Rieppel O.** 1991.Things, taxa and relationships. *Cladistics* 7(1): 93-100 DOI: 10.1111/j.1096-
502 0031.1991.tb00024.x.

503 **Rieppel O.** 2000. Sauropterygia I: Placodontia, Pachypleurosauria, Nothosauroidea,
504 Pistosauroidea. *Encyclopedia of paleoherpetology* 12: 1-134.

505 **Rosenthal HL, Eves MM, Cochran OA.** 1970.Common strontium concentrations of
506 mineralized tissues from marine and sweet water animals. C*omparative Biochemistry and*
507 *Physiology* 32(3): 445-450 DOI: 10.1016/0010-406X(70)90461-5.

508 **Sander PM.** 1989.The pachypleurosaurids (Reptilia: Nothosauria) from the Middle Triassic of
509 Monte San Giorgio (Switzerland) with the description of a new species. *Philosophical*
510 *Transactions of the Royal Society of London. B, Biological Science*s 325(1230): 561-666
511 DOI: 10.1098/rstb.1989.0103.

512 **Shinomiya T, Shinomiya K, Orimoto C, Minami T, Tohno Y, Yamada M.** 1998. In-and out-
513 flows of elements in bones embedded in reference soils. *Forensic science international* 98(1-2):
514 109-118 DOI: 10.1016/s0379-0738(98)00140-6.

515 **Scheyer TM, Klein N, Sander PM.** 2010.Developmental palaeontology of Reptilia as revealed
516 by histological studies. *Seminars in cell & developmental biology* 21(4): 462-470 DOI:
517 10.1016/j.semcdb.2009.11.005.

518 **Schroder AE, Rasmussen JA, Moller PR, Carnevale G.** 2022.Butyrumichthys henricii gen. et
519 sp. nov.: a new stromateiform fish from the lower Eocene Fur Formation, Denmark. *Journal of*
520 *Vertebrate Paleontology* 42(3): e2171798 DOI: 10.1080/02724634.2023.2171798.
521 **Tumarkin-Deratzian AR, Vann DR, Dodson P.** 2006. Bone surface texture as an ontogenetic
522 indicator in long bones of the Canada goose Branta canadensis (Anseriformes: Anatidae).
523 *Zoological Journal of the Linnean society* 148(2): 133-168 DOI: 10.1111/j.1096-
524 3642.2006.00232.x.
525 **Trueman CN, Palmer MR, Field J, Privat K, Ludgate N, Chavagnac V, Eberth DA, Cifelli**
526 **R, Rogers RR.** 2008. Comparing rates of recrystallisation and the potential for preservation of
527 biomolecules from the distribution of trace elements in fossil bones. *Comptes Rendus Palevol*
528 7(2-3): 145-158 DOI: 10.1016/j.crpv.2008.02.006.
529 **Trueman CN, Benton MJ.** 1997. A geochemical method to trace the taphonomic history of
530 reworked bones in sedimentary settings. *Geology* 25(3): 263-266 DOI:
531 10.1016/j.crpv.2008.02.006.
532 **Vitek NS, Vinther J, Schiffbauer JD, Briggs DE, Prum RO.** 2013.Exceptional three-
533 dimensional preservation and coloration of an originally iridescent fossil feather from the Middle
534 Eocene Messel Oil Shale. *Paläontologische Zeitschrift* 87: 493-503 DOI:
535 10.1007/s12542-013-0173-5.
536 **Vickram S, Rohini K, Srinivasan S, Nancy Veenakumari D, Archana K, Anbarasu K,**
537 **Jeyanthi P, Thanigaivel S, Gulothungan G, Rajendiran N, Srikumar PS.**2021.Role of zinc
538 (Zinc) in human reproduction: a journey from initial spermatogenesis to childbirth. *International*
539 *journal of molecular sciences* 22(4): 2188 DOI: 10.3390/ijms22042188.
540 **Wang Y-N, Fu W-L, Zhou M, Lu H, Sun Z-Y, Yao M-T, Jiang D-Y.** 2024. Micro X-Ray
541 Fluorescence technology reveals macrofossil bones and surrounding matrix element
542 characteristic—a case study of the Middle Triassic *Mixosaurus panxianensis*. *Spectroscopy and*
543 *Spectral Analysis*44(7):1974-1981 DOI: 10.3964/j.issn.1000-0593(2024)07-1974-08.
544 **Xue Y-F, Jiang D-Y, Motani R, Rieppel O, Sun Y-L, Sun Z-Y, Ji C, Yang P-F.** 2013.New
545 information on sexual dimorphism and allometric growth in *Keichousaurus hui*, a
546 pachypleurosaur from the Middle Triassic of Guizhou, South China. *Acta Palaeontologica*
547 *Polonica* 60(3): 681-687 DOI: 10.4202/app.00006.2013.
548 **Young C-C.** 1958. On the new Pachypleurosauroidea from Keichow, South-West China. *Ver.*
549 *PalAsiat.* 2, 69–81.

Figure 1

Fig.1 Regression of the body size (proxy : humeral midshaft circumference) on the age of *K. hui* (R^2 :0.86124) (modified based on data from Li et al. 2023), with three specimens superimposed.

The plots of our examined specimens show that XNGM WS-30-R43, GMPKU-P-4316, and XNGM WS-32-R18 are juvenile, subadult and adult, respectively.
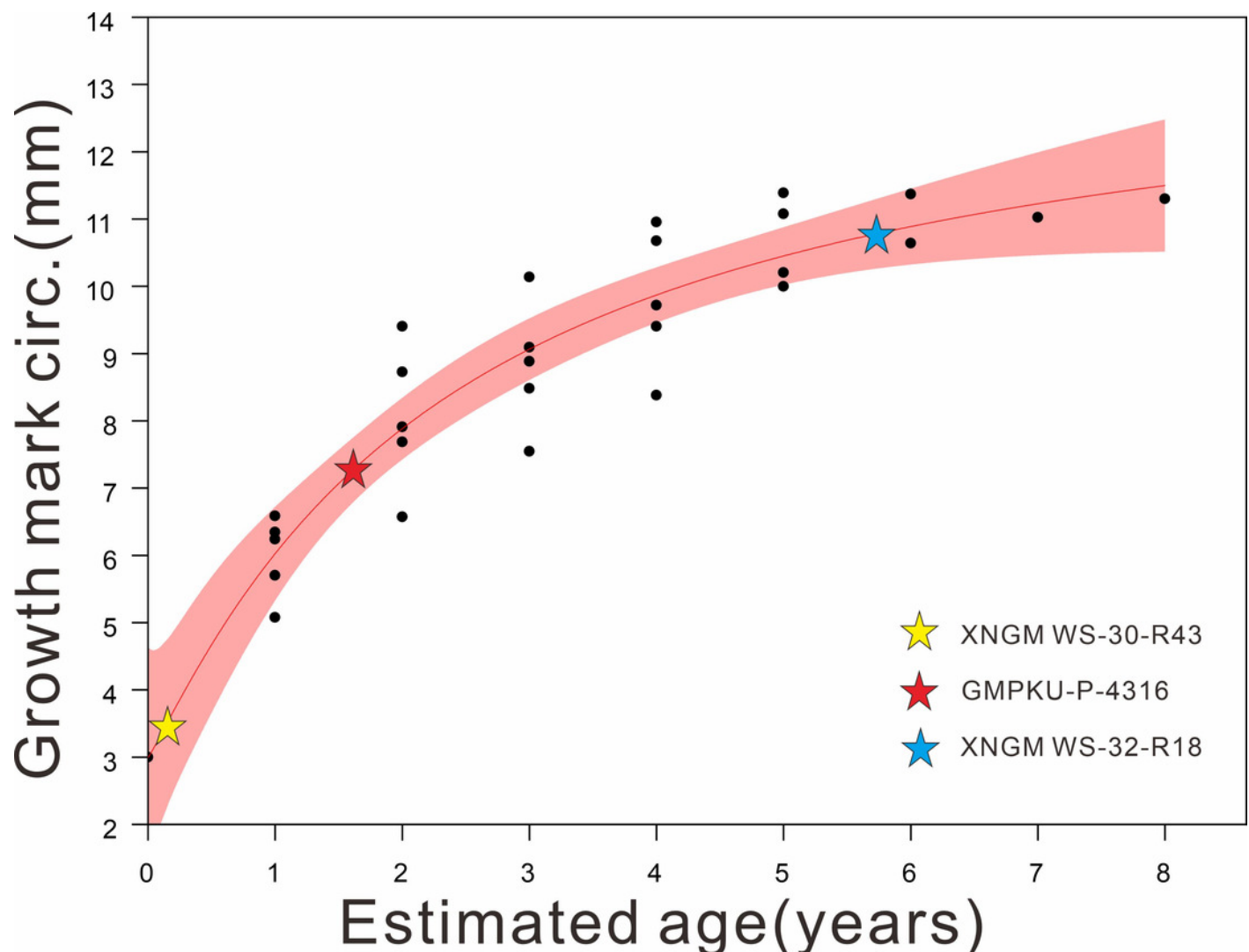
Figure 2

Fig.2 Elemental distribution map and drawing of XNGM WS-30-R43.

(A) Photo of XNGM WS-30-R43. (B)-(E)Micro-XRF maps (false-color images) of Ca(B), P(C), Sr(D), Zn(E). (F) Drawing of XNGM WS-30-R43 and distribution diagram of Zn. The scale bars are 20 mm.
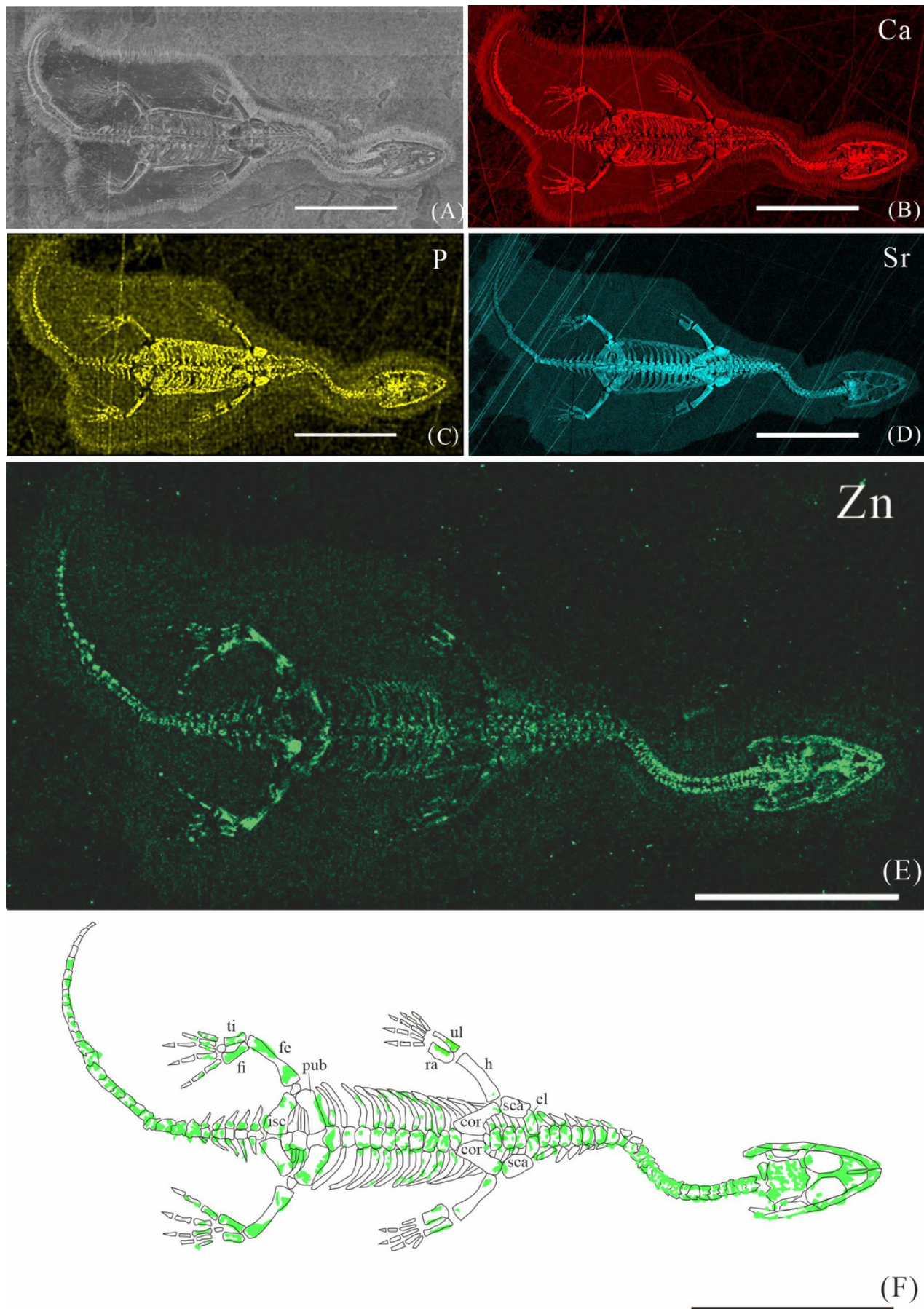
Figure 3

Fig.3 Elemental distribution map and drawing of GMPKU-P-4316 .

(A)Photo of GMPKU-P-4316. (B)-(E)Micro-XRF maps (false-color images) of Ca(B), P(C), Sr(D), Zn(E). (F)Drawing of WS-30-R43 and distribution diagram of Zn. The scale bars are 3 cm.
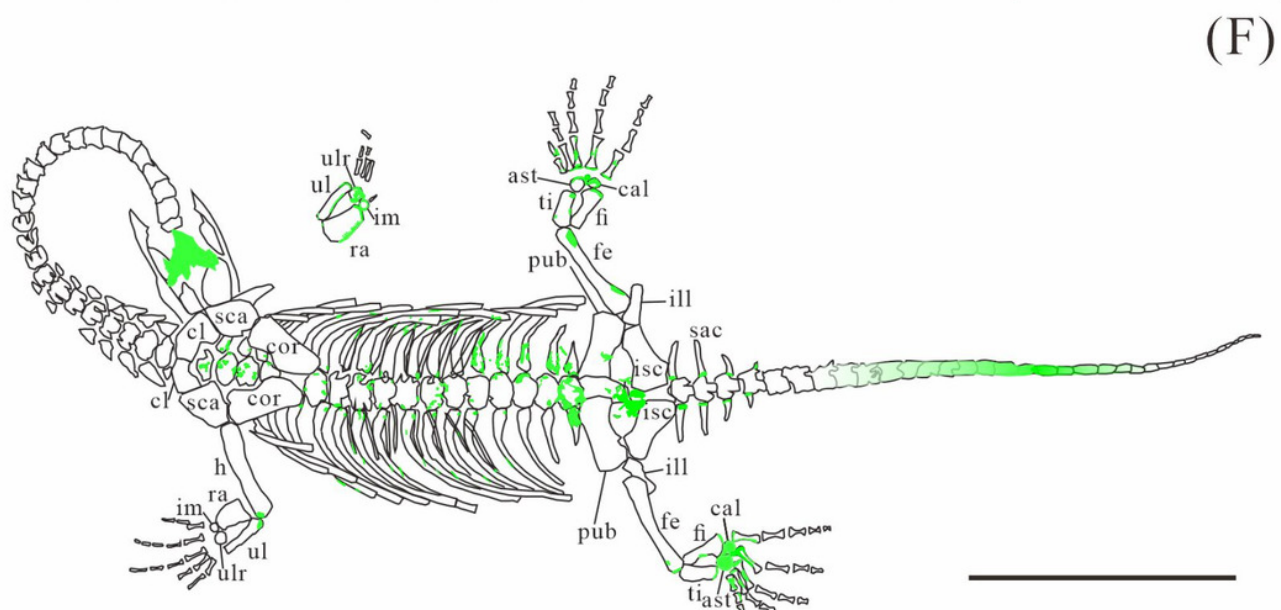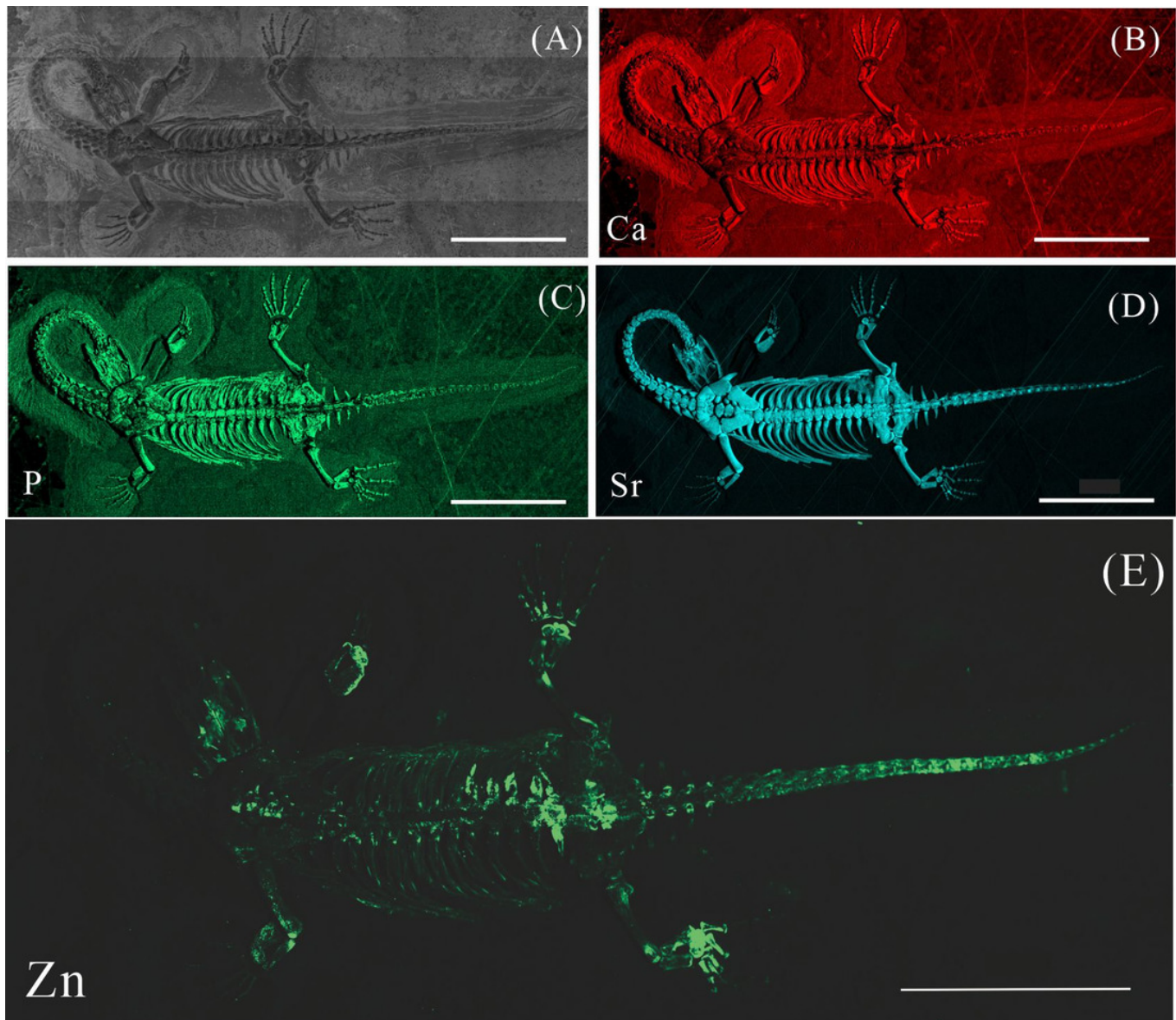
Figure 4

Fig.4 Elemental distribution map and drawing of XNGM WS-32-R18.

(A)Photo of XNGM WS-32-R18. (B)-(E)Micro-XRF maps (false-color images) of Ca(B), P(C), Sr(D), Zn(E). (F)Drawing of WS-30-R43 and distribution diagram of Zn. The scale bars are 4 cm.

(A)

Ca (B)

P (C)

Sr (D)

Zn (E)

(F)
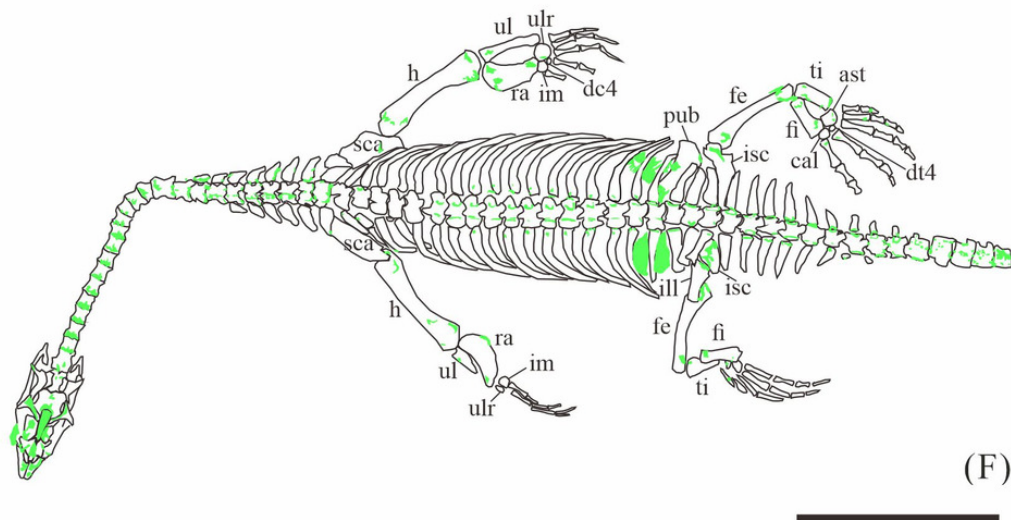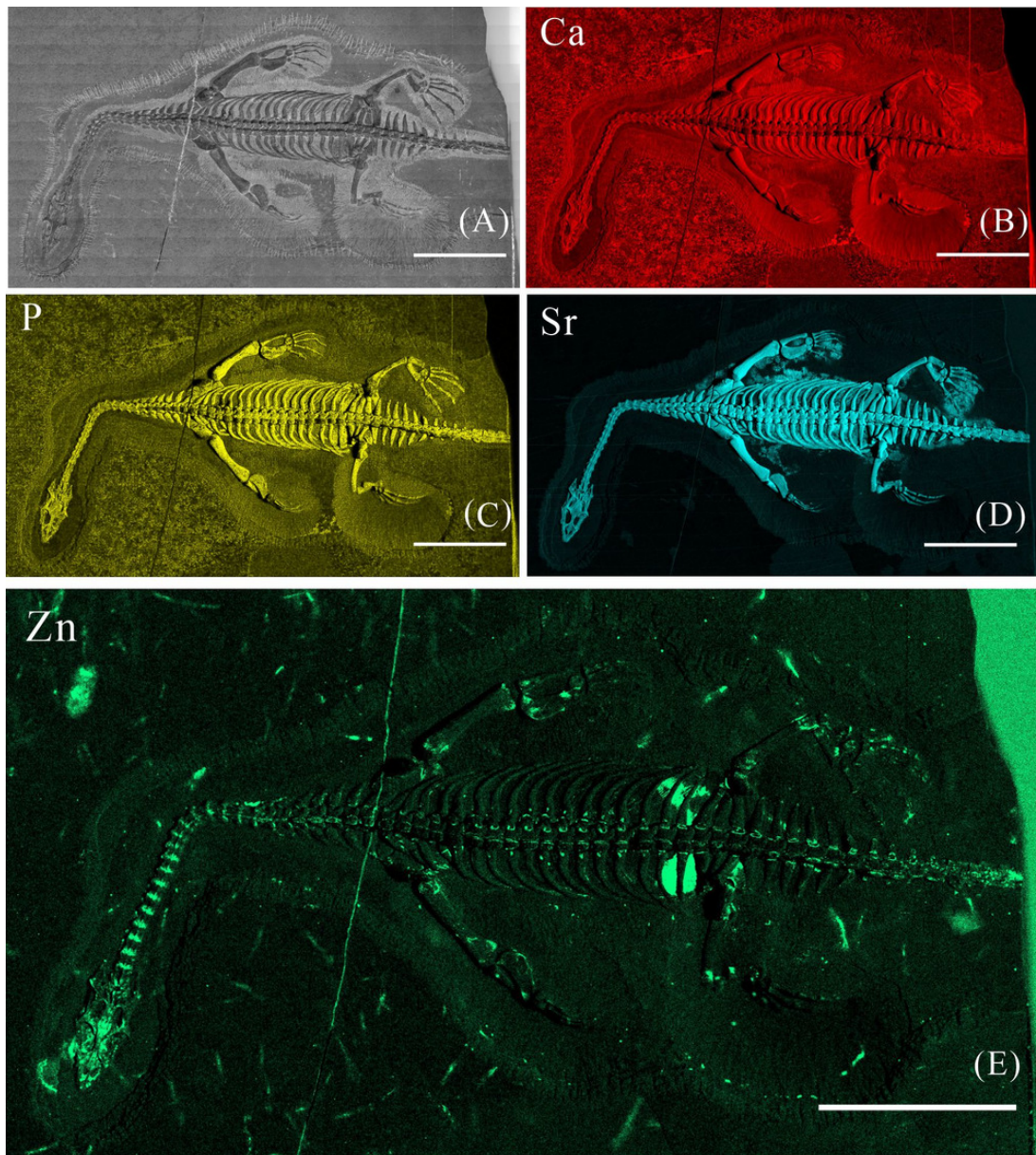
Figure 5

Fig.5 The ossification pattern in *Keichousaurus hui*.

(A)the different bone development patterns in juvenile and subadult individuals. (B) the ossification pattern of tarsus in *Keichousaurus hui*.
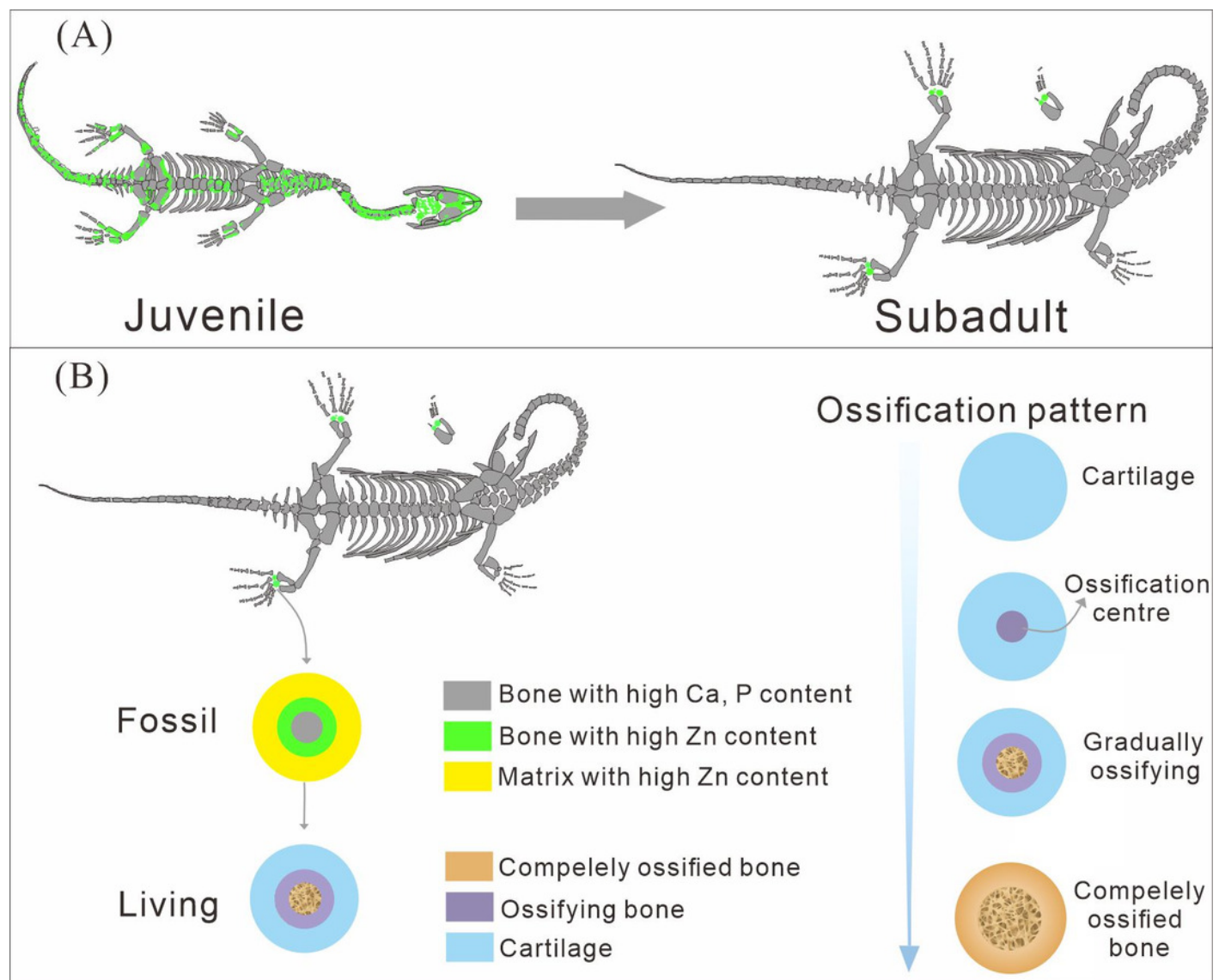
Figure 6

Fig.6 Elemental distribution map and drawing of GMPKU-P-4316's left hindlimb.

(A) the position of left hindlimb. The scale bar is 3 cm. (B) Photo of GMPKU-P-4316's left hindlimb. The scale bar is 3 mm. (C)-(F)Micro-XRF maps (false-color images) of Ca(C), P(D), Sr(E), Zn(F). The scale bars are 3 mm. (G) drawing of GMPKU-P-4316's left hindlimb. (H)-(K) the drawing of different elemental distribution, Ca(H), P(I), Sr(J), Zn(K). (L) the distribution of Zn and Ca in GMPKU-P-4316's tarsal. The scale bar is 1 mm. (M) the distribution of Zn and P in GMPKU-P-4316's tarsal. The scale bar is 1 mm. (N) the distribution of Zn in GMPKU-P-4316's astragalus, calcaneum, and the dt4. The scale bar is 0.5 mm.
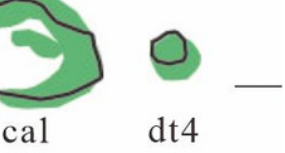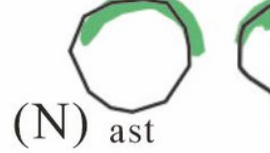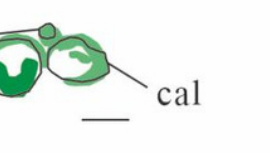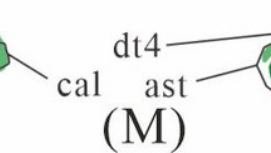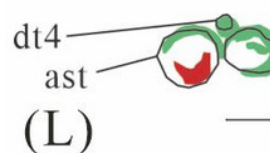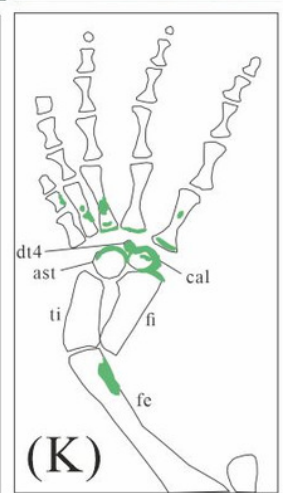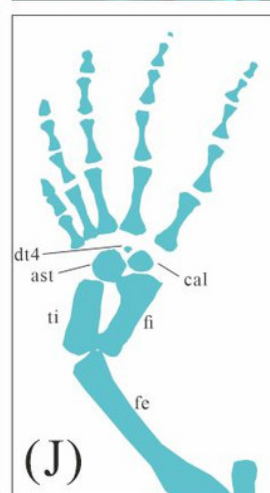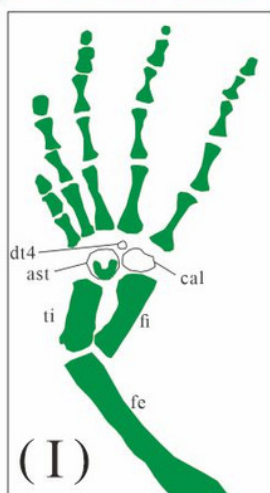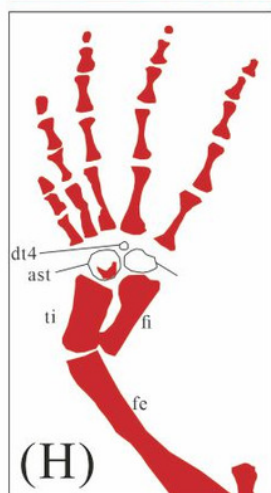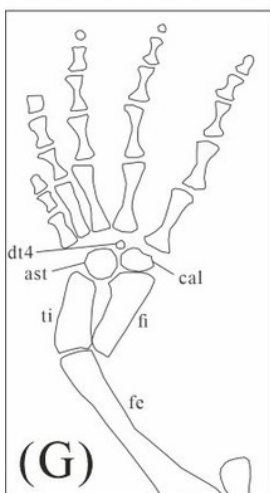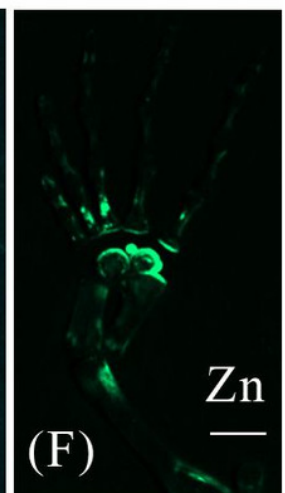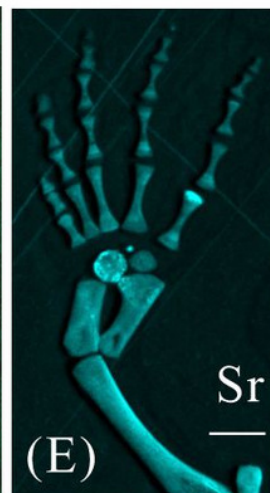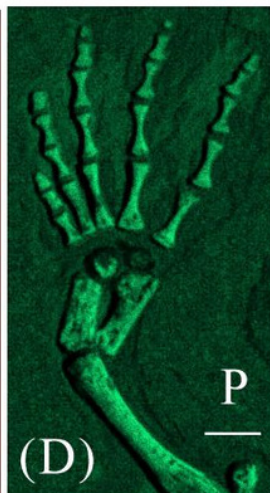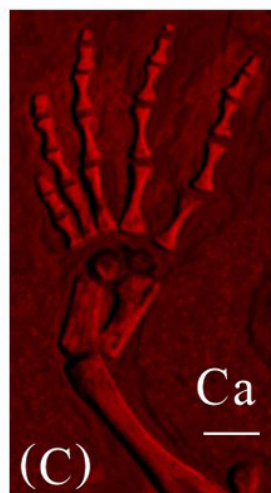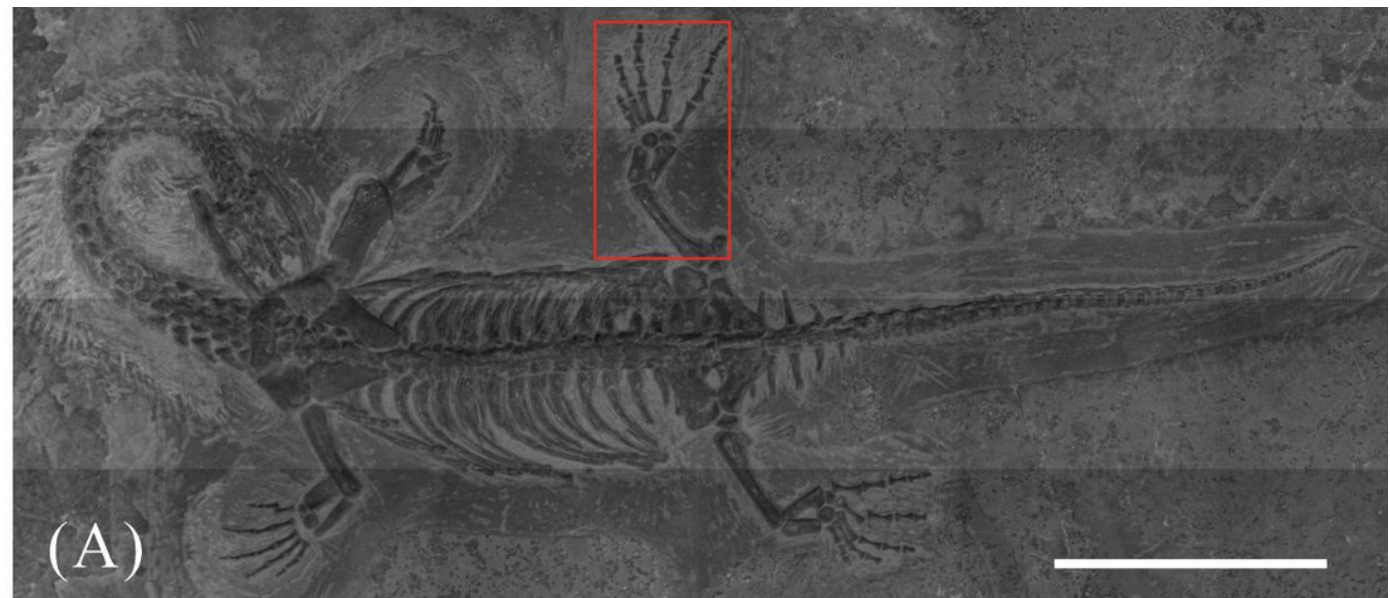
Figure 7

Fig.7 Elemental distribution map and drawing of GMPKU-P-4316 right hindlimb.

(A) the position of the right hindlimb. The scale bar is 3 cm. (B) Photo of GMPKU-P-4316's right hindlimb. The scale bar is 5 mm. (C)-(E), (j)Micro-XRF maps (false-colour images) of Ca(C), P(D), Sr(E), Zn(J). The scale bars are 5 mm. (F) drawing of GMPKU-P-4316's right hindlimb. (G)-(I), (K) the drawing of different elemental distribution, Ca(G), P(H), Sr(I), Zn(K). (L) the distribution of Zn and Ca in GMPKU-P-4316's tarsal. The scale bars are 2 mm. (M) the distribution of Zn and P in GMPKU-P-4316's tarsal. The scale bar is 2 mm.(N) the distribution of Zn in GMPKU-P-4316's astragalus, calcaneum, and dt4. The scale bar is 1 mm.

(A)

(B) (C) Ca (D) P (E) Sr

(F) fe fi cal ti ast (G) fe fi cal ti ast (H) fe fi cal ti ast (I) fe fi cal ti ast

(J) Zn dt4? (L) cal ast (M) cal ast (N) ast cal dt4
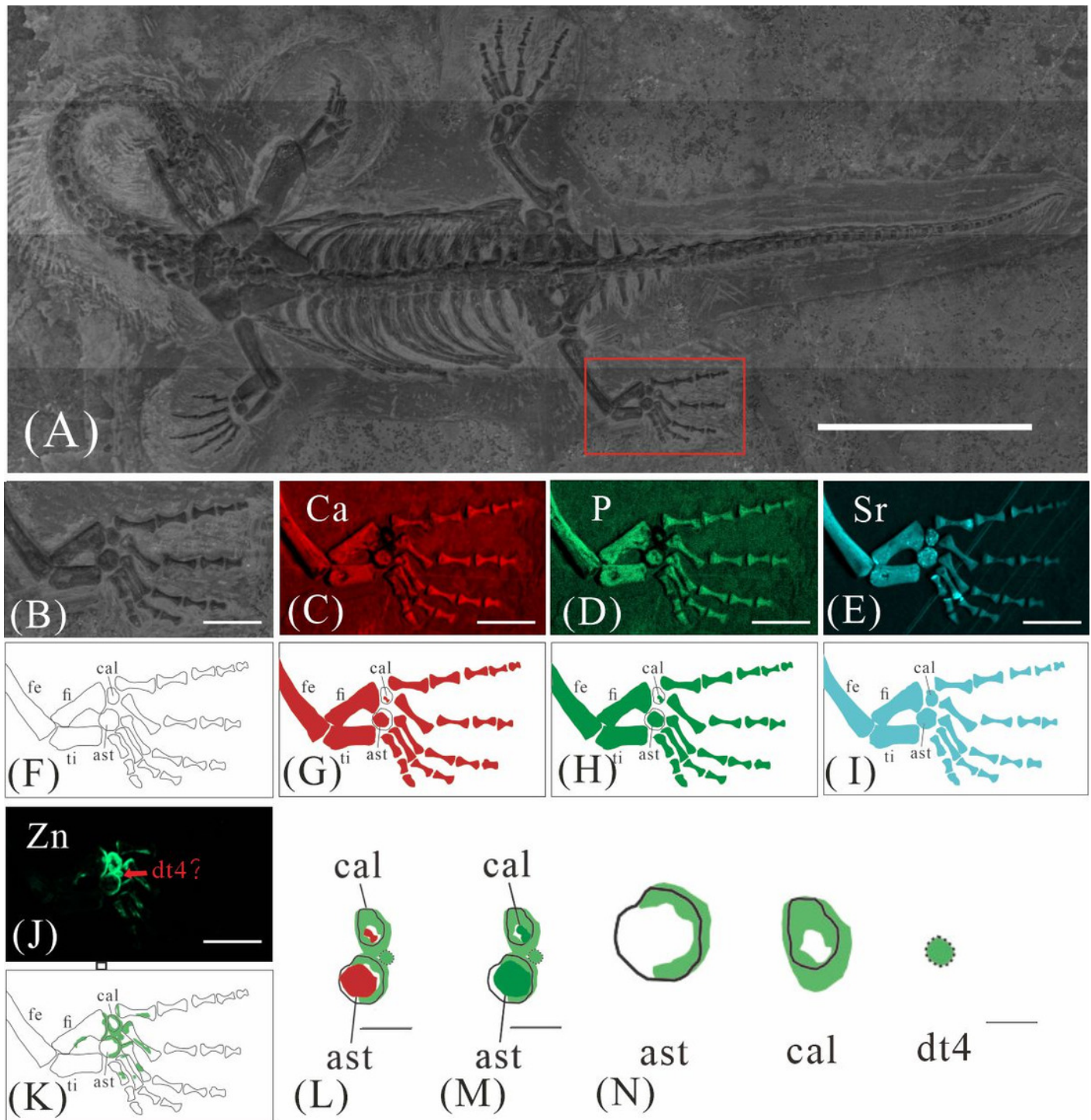
(K) fe fi cal ti ast

Figure 8

Fig.8 Comparison of limb ossification between *Keichousaurus hui*, extant reptile and mammal.

(A), (E) the distribution of Zn in GMPKU-P-4316's carpal and tarsal, respectively. (B), (F)the cartilage and bone in the carpal and tarsal of *Cyrtodactylus pubisulcus*, respectively (modified from Rieppel, 1992). (C), (G) the cartilage and bone in the carpal and tarsal of mouse (modified from Patton & Kaufman, 1995). (D) the distribution of Zn in mouse (modified from Anne et al., 2017).
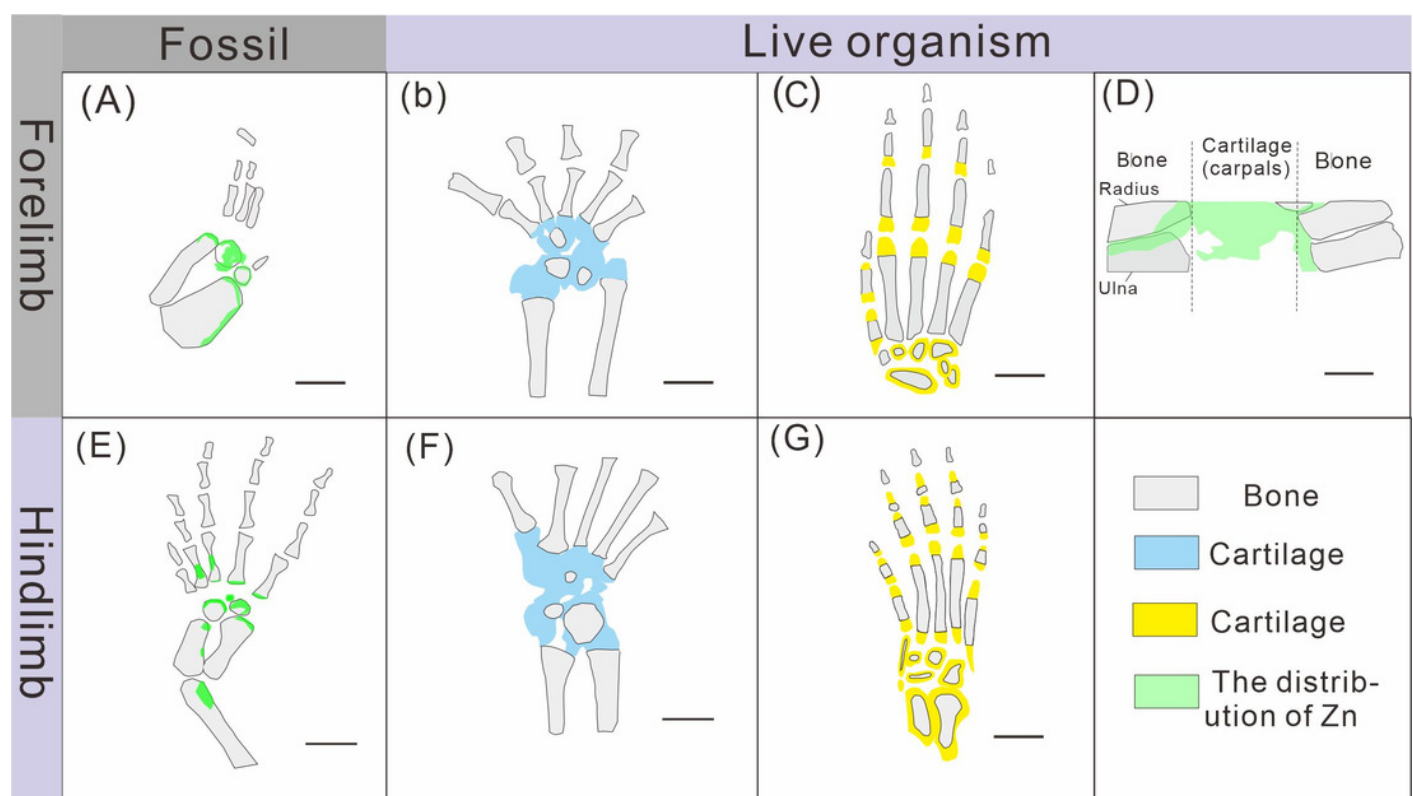
Table 1(on next page)

Table1 Measurements of the skeleton in *Keichousaurus hui* (mm)

SN, specimen number; HL, humerus Length; MAXDWH, maximum distal width of humerus;

MINWHS, minimum width of humeral shaft; HMC, humeral midshaft circumference; FeL,

femur length; SVL, snout-vent length; SL, standard length; OS, ontogenetic stage; G, gender.

1 **Table1 Measurements of the skeleton in *Keichousaurus hui* (mm)**

2

SN	HL	MAXDWH	MINWHS	HMC	FeL	SVL	SL	MAXDWH/MINWHS	HL/FL	HL/SL	OS	G
XNGM-WS-31-R22	4.45	-	-	-	4.78	45.72	4.37	-	0.93	1.02	-	-
XNGM-WS-32-R43	5.85	1.76	1.09	3.42	6.82	59.54	5.28	1.62	0.86	1.11	juvenile	-
GMPKU-P-1154(2)	7.40	2.17	1.26	3.96	8.40	88.43	7.43	1.72	0.88	1.00	juvenile	-
GMPKU-P-4316	11.62	2.93	2.26	7.10	11.94	117.61	10.57	1.30	0.97	1.10	subadult	-
GMPKU-P-4317	17.52	4.21	3.24	10.17	16.75	167.97	—	1.30	1.05	-	adult	female
GMPKU-P-4318	22.26	5.27	3.67	11.52	20.67	166.28	17.38	1.44	1.08	1.28	adult	female
XNGM-WS-32-R18	26.44	6.57	3.48	10.92	21.20	178.74	15.82	1.89	1.25	1.67	adult	male

3

4 SN, specimen number; HL, humerus Length; MAXDWH, maximum distal width of humerus;

5 MINWHS, minimum width of humeral shaft; HMC, humeral midshaft circumference; FeL,

6 femur length; SVL, snout-vent length; SL, standard length; OS, ontogenetic stage; G, gender.